Combination of robust point measurement techniques on the vortex tube: FRS, DGV and L2F deliver thermodynamic and flow properties

Eike J. Burow*, Manfred Beversdorff, Guido Stockhausen, Michael Schroll, Christian Willert
Institute of Propulsion Technology, German Aerospace Center (DLR), Germany
* Correspondent author: eike.burow@dlr.de

Keywords: FRS, DGV, L2F, Point measurements, Ranque-Hilsch vortex tube

ABSTRACT

High-end laser-optical measurements on industrial applications are often restricted to optical access via endoscopes. Since usually no single technique is able to all relevant variables of major technical flows, there is great interest in complemental combinations. This contribution presents a single-point approach to joining Filtered Rayleigh Scattering (FRS) with Doppler Global Velocimetry (DGV) and Laser-2-Focus (L2F): while L2F delivers two velocity components, temperature and pressure data are supplied by FRS. The third velocity component is added by both DGV and FRS. To put this vision into effect, measurements of all three techniques are conducted on a uniflow Ranque-Hilsch vortex tube using the same hardware: since the system has been originally designed for 3c-L2F the main focus is on the addition of FRS. While measurement results are validated literature sources and additional PIV reference data, challenges and solutions of the system setup as well as data evaluation methods are discussed: although calibrated numerical models for Rayleigh scattering spectra can be used to incorporate systematic deviations, the physically well-founded Tenti-S6-model once again proves to deliver accurate output under tough conditions. As a main result it is found that fluorescence background is emerging from signal fibers: strong Mie scattered light originating from particles needed for L2F and DGV may excite a fused silica fiber and produce broadband luminescence. Since this occurs before the FRS-typical powerful background filtering, it leads to disruptive cross-talk on the considerably lower FRS signal. Solving this issue promises simultaneous measurements of particle and fluid velocity, allowing slip analysis.

1. Introduction

Applications of laser-optical measurement techniques on industrial technical flows more often than not come with severe limitations, such as limited optical access, window pollution, harsh environments or strong noise and vibrations. While fundamental research often allows experiments with generous optical access, this contribution is focused on single-access and single-point techniques for endoscopic use. Individually these rarely deliver all of the required information, so there is great interest in complemental combinations. While research projects on the one hand come with demands on the measured properties, methods have to be selected and tested to work well on the same hardware as well as on the same measurement schedule:

Filtered Rayleigh Scattering (FRS; Forkey, 1996), Doppler Global Velocimetry (DGV; Meyers, 1991) and Laser-2-Focus (L2F; Schodl, 1980) are now tested towards their compatibility. L2F and DGV have already been proven to work well with each other (3c-L2F; Röhle, 1999): while L2F delivers two velocity and turbulence components, DGV - applied in a particle-wise discretized version compatible to L2F electronics - adds the third component. Most promising however is the addition of FRS, adding mean values of temperature and pressure. While FRS requires additional hard- and software, this will also be used in the future to implement an integrating and frequency scanning version of DGV, since the discretized version severely suffers from background noise.

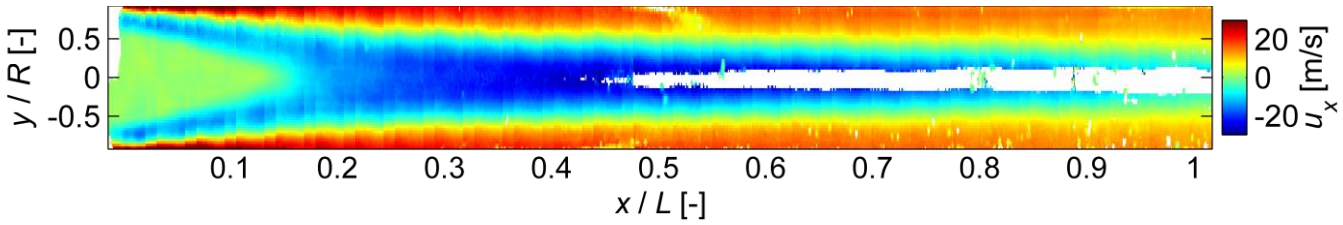

Fig. 1 The flow field of a uniflow vortex tube (Burow, 2016) serves as a starting point for the presented research.

As a development platform for testing and evaluation a Ranque-Hilsch vortex tube (RHVT) is used. As already presented in the context of Particle Image Velocimetry development (PIV; Raffel, 2018), the vortex tube offers a complex though reproducible three-dimensional flow field, well suited as a reference experiment for rotating flows (Burow, 2016). While used in a uniflow configuration, the internal flow field (Fig. 1) has been shown not to differ qualitatively from a typical RHVT featuring a second outlet, which provides a variety of interesting flow phenomena including aspects of heat- and mass transfer, turbulence and thermoacoustics (Xue, 2010), invoking Maxwell's Demon and resulting in a spatial temperature separation (Liew, 2012). These aspects however are outside of the focus of this contribution and will not be discussed in detail.

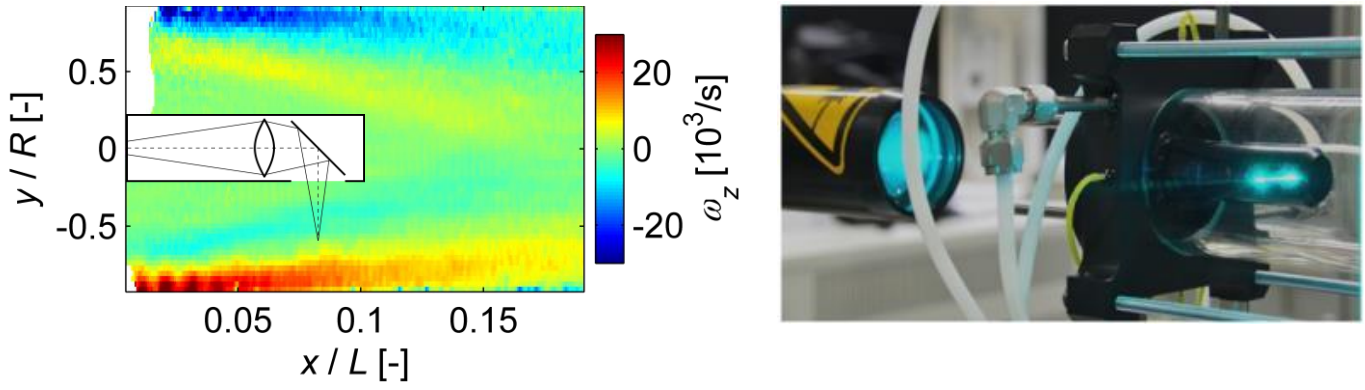

Fig. 2 To enable measurements from within the vortex tube, a mirror was introduced held by an axial tube. This way the countercurrent can be measured at its reversal point (sign change of vorticity $\omega_z = \partial u_y/\partial x - \partial u_x/\partial y$, left).

To be able to evaluate measurements of an axial velocity component u_x in the presence of a larger tangential velocity (expectedly about 5 times at the given length-to-diameter ratio $L/D \sim 25$ of the RHVT) from the center (as it shall be done in a later step with an endoscope) a tube with a diameter of 20mm containing a mirror is integrated within the inlet-sided solid body rotation area (Fig. 2, left), where the disturbance of the flow field is expected to be minimal. For this purpose the original vortex tube design was scaled by a factor of two ($D = 60$ mm, $L = 1.5$ m).

2. Methods and Experimental setup

Besides the scaling and the mirror tube the RHVT is set up in a similar manner to (Burow, 2016): on the left end the operating material - air or sulfur hexafluoride SF_6 - is introduced tangentially through four critical nozzles at $x = 0$, resulting in a strong circulation (ref. Fig. 3). The gas precesses turbulently through the tube towards the outlet on the right, which has the shape of a circular slit, formed by an adjustable cone and the tube end: the slit width is set for a pressure difference of 85 hPa to degenerate the tube from exterior asymmetries. After this point the gas is circulated, for particle-based measurements (L2F, DGV) it is led through a seeding generator.

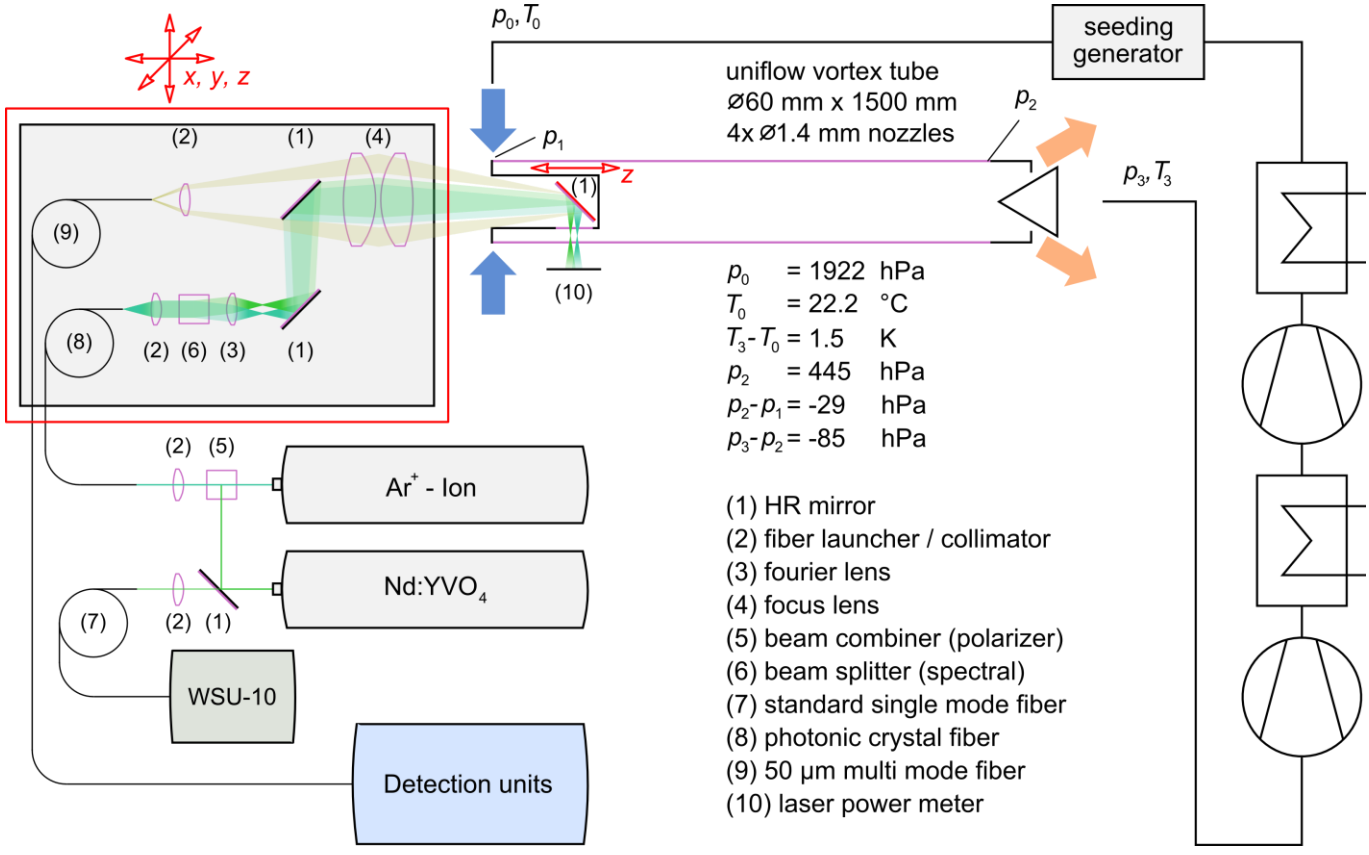

Fig. 3 The same optics are used for FRS, DGV and L2F, changing only the detection unit: while the inner part of the focus lens' aperture (4) is used for illumination, the outer part collects scattered Rayleigh and Mie signal.

The measurement volume is defined by the beam waist of the illumination optics; since the same configuration is used for detection as well, geometrically scattered and other false light is filtered spatially by the diameter of the detection fiber, which basically works as a mode aperture. By traversing the optical head towards the fixed mirror within the RHVT, the beam waist is traversed radially; by moving the optics together with the mirror it is traversed axially to one of four windows. Axial measurement points are located $x = (0.25\ 0.5\ 0.75\ 1) \cdot D$, radial positions at $r = (0.225\ 0.275\ 0.325\ 0.375\ 0.425\ 0.475) \cdot D$.

Laser-2-Focus

The underlying optics were originally designed for 3c-Doppler-L2F. Since it has been used successfully in similar configuration before on a regular basis (e.g. Förster, 2000), in this work they are basically used 'as is' with a focus on FRS adaptations; a short introduction into the workings of L2F however is in order nonetheless to understand the system architecture. Laser-2-Focus, as the name suggests, is based on two spatially separated beam waists forming a sensor barrier: the Mie signal of a particle crossing a waist results in a temporal peak on a photomultiplier tube (PMT). Correlating the PMT signal of both waists with known spatial distance tells the portion of particles crossing both waists; thus by rotating the foci towards the maximum correlation value the direction of the velocity vector is determined within a plane orthogonal to laser propagation, while its value results from the temporal shift. Additional anisotropic turbulence information can be calculated from the width of the correlation peaks along temporal and angular axes.

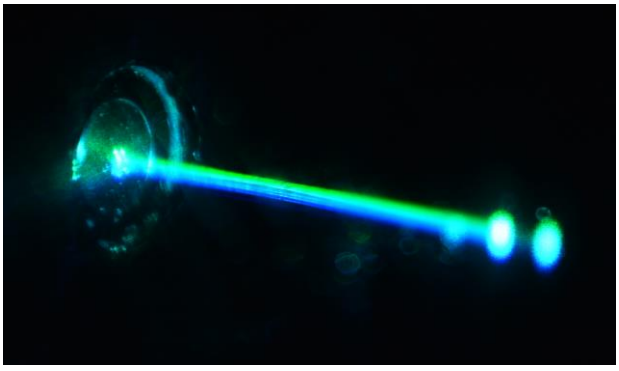

Fig. 4 L2F is based on discrete seeding particles crossing two spatially separated spectral laser foci (center). The beams are introduced into the seeded RHVT through one of the windows in the mirror tube (left).

To produce these two foci an Argon-ion laser is used in combination with a rotatable spectral beam splitter/prism (Fig. 3, (6)), the distance of the foci is then determined by the selection of laser lines (Fig. 4). Choices are made in respect to the trade-off between local distinction (higher focus distance → more averaging), turbulent correlation loss (lower portion of particles crossing both waists) and dynamic range (higher temporal shift → lower measurement uncertainty).

Doppler Global Velocimetry

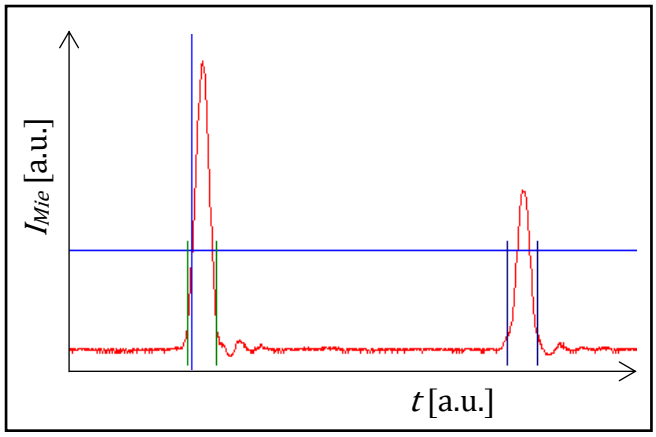

Fig. 5 Contrary to L2F for the Doppler part the peaks are evaluated quantitatively - as long as they are distinguishable from each other and from background noise.

The third velocity component (along the probe axis) is measured additionally via DGV: an additional laser line from a frequency stabilized Nd:YVO_4-Laser (Coherent Verdi V6) is coupled into the measurement volume; its frequency is tuned to a distinct molecular absorption feature of iodine using a HighFinesse Wavelength-meter WSU-10. The signal from this (third) focus is separated spectrally and relayed to its own PMT twice: once directly (reference), once delayed temporally by an additional fiber ($\Delta t = L_{fiber} \,/\, c_L$ with $L_{fiber} = 200$ m) and filtered by the iodine cell (signal). While the temporal distance of these two signals is fixed (Fig. 5), the ratio of their integrals translates (via a calibrated look-up table) to the iodine absorption depending on the frequency of the signal and hence the Doppler shift $\Delta\nu$ resulting from particle movement $\vec{u}$: $\Delta\nu = \nu_{0,Laser} \,/\, c_L \cdot \vec{u} \cdot (\overrightarrow{e_O} - \overrightarrow{e_L})$, where $\overrightarrow{e_O}$ and $\overrightarrow{e_L}$ are unit vectors in directions of observation and laser illumination respectively. The presented backward scattering is defined by $\overrightarrow{e_O} = -\overrightarrow{e_L}$.

This particle-wise method is known to be limited close to walls - or in this case even the AR-coated glass of the vortex tube - due to limited mode filtering in laser propagation direction, resulting in a low signal-to-background ratio up to the point where single particle peaks are indistinguishable: for once the dynamic range of the PMT is occupied by the background, but most of all even small relative variations of a large background signal dominate a smaller signal level. Because of this a temporally integrating and frequency scanning approach is tested: instead of resolving single particles at one single laser frequency, the filtered signal is integrated for 3 seconds per laser frequency; frequency is then scanned along the flank of an iodine absorption feature (cell saturation temperature of 70°C, cell length of 50 mm). The resulting Mie signal is a shifted mirror image of the absorption flank (Fig. 6): the frequency shift - related to velocity - as well as a constant background level and seeding density and even line deformation by turbulence may be evaluated by nonlinear regression. Laser intensity fluctuations are measured either by an unfiltered reference diode within the detection unit (analogue to the 3c-L2F hardware described above) or - accessibility provided - by a detector within the

measurement area (Fig. 3, (10)). Other significant variations of key parameters during the scan however would cause problems during evaluation: velocity, turbulence, background level, seeding density and window staining impacting the laser power measurement.

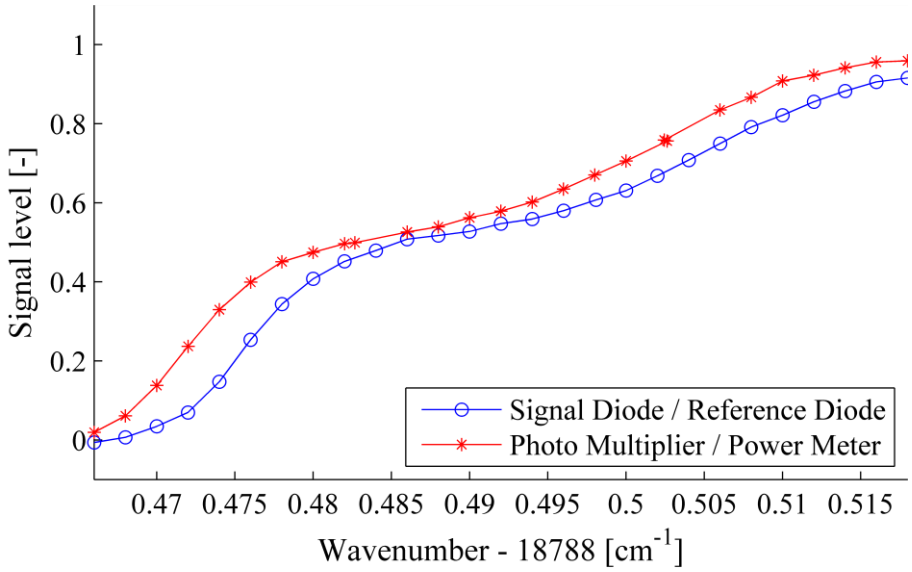

Fig. 6 Preliminary tests of scanning DGV on a free expanding jet: the Doppler shift between both measurements is clearly visible. Signal and reference diodes (Thorlabs DET 36A) are compared to a PMT (Hamamatsu H9305-04) using a coherent laser power meter for scaling: both setups perform similarly under the given conditions.

Filtered Rayleigh Scattering

The employed Frequency Scanning Method (FSM) of FRS is based on the works of (Doll, 2016). Based on light scattered elastically by molecules FRS is a seeding-free method. The spectral response of single-frequency illumination (e.g. Fig 7, colored curves) contains information about temperature and pressure (Laser Rayleigh scattering; Miles 2001): a single photon scattered by a single molecule is Doppler shifted by its thermal movement the same way as described before in the context of DGV. In a continuous fluid the Maxwell-Boltzmann-distribution of thermal movement results in Gaussian broadening of the detected spectrum related to the fluid temperature. Additional Loretzian line properties result from pressure dependent acoustic sidebands (Brillouin scattering). Thus by comparing a measured Rayleigh spectrum (RS) to a suitable theoretical model (e.g. Tenti, 1974) temperature and pressure can be extracted. Also bulk movement of the fluid movement results in a measurably Doppler shifted spectrum.

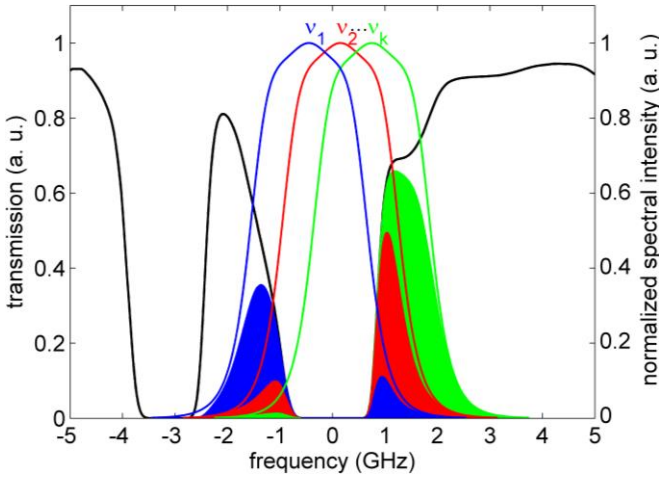

Fig 7 While most sensors lose all spectral information due to integration, the frequency scan returns the required uniqueness (Doll, 2014).

Experimental conditions of technical flows however usually exclude the use of spectral detectors such as spectrometers or etalons for direct analysis of the RS: on the one hand unshifted laser light from particles and geometric elements (walls, windows, beam traps, …) may dominate the weaker RS by about three to five orders of magnitude, on the other hand planar measurements or weak signal levels may restrict the detector options. This is where FRS comes into play: the illuminating laser source is tuned to a molecular absorption feature; in this case again a Verdi V6 is measured, stabilized and tuned by a HighFinesse WSU-10, supported by National Instruments DAQ hardware. If observed through the absorption spectrum of said iodine cell (T = 70°C, L = 50 mm; Fig 7, black curve) unshifted background light is filtered effectively, also the Rayleigh spectrum is multiplied with the absorption (colored areas) and then integrated by the detector (Hamamatsu H9305-04 PMT). To retain the required spectral information the laser frequency is scanned along the iodine feature: the resulting scan curve (such as in Fig 8) represents the convolution between the absorption spectrum and the Rayleigh spectrum. This is evaluated towards temperature, pressure and mean velocity by nonlinear regression against iodine cell calibration data and the Rayleigh model.

The chosen Rayleigh model has a strong influence on overall measurement uncertainties. While the Tenti S6 model is derived directly from physics and has been shown to accurately calculate Rayleigh spectra, often a calibrated analytical model (Doll, 2016) better represents data from a complex measurement setup, incorporating some spectral effects of used optics and devices. Here an analytical model will be calibrated for SF_6 based on calibration data acquired on the same setup as the measurement data, comparing its evaluation results to those of the Tenti S6 model.

The hardware in Fig. 3 is used for FRS as well; the detection unit consists of a lens, imaging the fiber exit on the PMT through the iodine cell and a narrow bandpass filter (Thorlabs FLH532-4). Including FRS into endoscopic hardware may result in side effects. One known perturbation is the fluorescence of the much stronger Mie light within signal fibers:

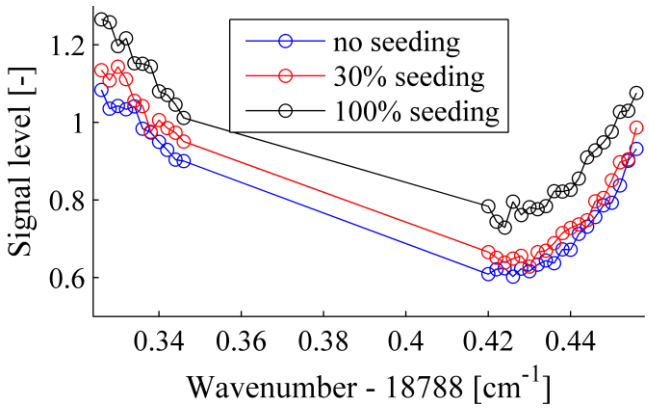

Fig 8 Preliminary FRS scans on a free expanding jet in the presence of different amounts of seeding shows some residual influence of Mie scattering.

while the narrowband Mie light itself is eliminated afterwards by the iodine cell, which is scanned over a range featuring a transmission $\tau < 10^{-5}$, the broadband fluorescence of the fiber will be transmitted partially. While this effect is mostly encountered on image fiber bundles (Udovic, 2008), preliminary FRS scans in the presence of strong seeding show similar behavior of the used 50µm multimode fiber (Fig 8): depending on the seeding level ('no seeding' still means significant Mie scattering due to residual particles within the tubing) a distinct background level is encountered, which may or may not be corrected during evaluation, depending on its progression during the FRS scan.

Another known effect is a change in the overall transmission efficiency R of illumination and observation beam paths after its determination via a reference scan. With R unknown quantitative intensity measurements are impossible; by normalizing the entire FRS scan however an evaluation of p, T and u is still possible (combined method). This was originally encountered on an RHVT, where activation of the flow resulted in a refractive index gradient redistributing the laser light used for illumination (Doll, 2015). While retaining temperature and velocity information, this way however the measurement uncertainty of pressure data is greatly increased: any density information relating to pressure via ideal gas law is lost.

3 Results

The first concern when combining molecular FRS with seeding-based L2F is the effect of Mie scattered light on the FRS measurement - most of all said fluorescence within the signal fiber induced by Mie scattering. Thus data from a free expanding jet as shown in Fig. 8 are evaluated using the Tenti S6 model. The relative residual R_s (Doll, 2016) of a FRS scan with frequencies f, describing the deviation between modelled ($S_{f,mod}$) and measured ($S_{f,meas}$) data points, serves as a key indicator for data quality:

$$R_s = \sqrt{\frac{\sum_f (S_{f,mod} - S_{f,meas})^2}{\sum_f S_{f,meas}{}^2}}$$

When evaluating the measurement without extra seeding (Fig 9; only some residual seeding in the tubing), the overall residual of 2% indicates a major fault (successful evaluations usually exhibit $R_s < 1.5\%$, with $R_s < 0.6\%$ indicating excellent convergence). Also when looking at its distribution over the FRS scan (bottom, bar plot) it is obviously not only based on shot noise but some systematical deviation. The fitted background C_t of 21% (related to the modelled Rayleigh signal) also indicates significant Mie cross-talk. In the end however when looking at the difference between measured and actual (as calculated isentropically for the free expanding jet) temperature ΔT, pressure Δp and projected velocity Δu the data are found to be totally off (ΔT = 60 K, Δp = 28 mbar, Δu = -6 m/s).

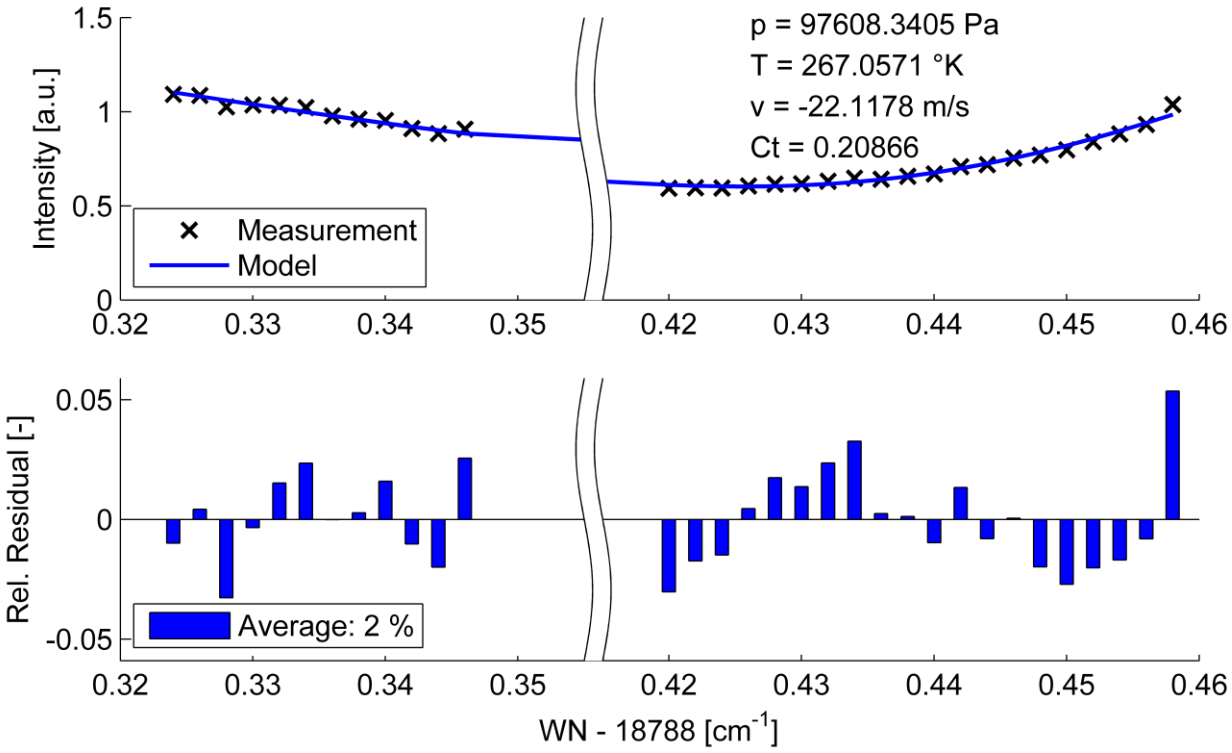

Fig 9 Seeding induced fluorescence within the signal fiber results in a systematic background rendering the corresponding data useless for FRS evaluation.

Evaluation of measurements with significant additional seeding (30%, 100% setting) however show similar error ranges ($|\Delta T| < 60$ K, $|\Delta p| < 170$ mbar, $|\Delta u| < 8$ m/s with $R_s > 1.8$ %). Considering this there may have been some alignment issues within the complex setup as well, suggesting a detailed investigation of this subject in a more methodical approach.

The second concern is whether or not the transmission efficiency of the entire optical system is sufficiently constant to allow quantitative evaluation of the data. Thus acquired data from the vortex tube are evaluated and compared using the standard FSM as well as the combined method; with $\overrightarrow{e_O}$ and $\overrightarrow{e_L}$ both directed radially so is the measured velocity component. The exemplary data set at $x = 0.5 \cdot D$, $r = 0.425 \cdot D$ (SF_6, Tenti) results in $T = 297.0$°K, $p = 423$ mbar, $u_{rad} = 1.9$ m/s using standard FSM (Fig. 10) and $T = 297.3$°K, $p = 427$ mbar, $u_{rad} = 1.9$ m/s using the combined method. All in all the deviations are well within expected measurement uncertainties, thus with the exception of single points close to the tube ($r = 0.475 \cdot D$), quantitative evaluation by standard FSM is applicable. Residuals of 1.2% for both FSM and combined method also lead towards FSM evaluation.

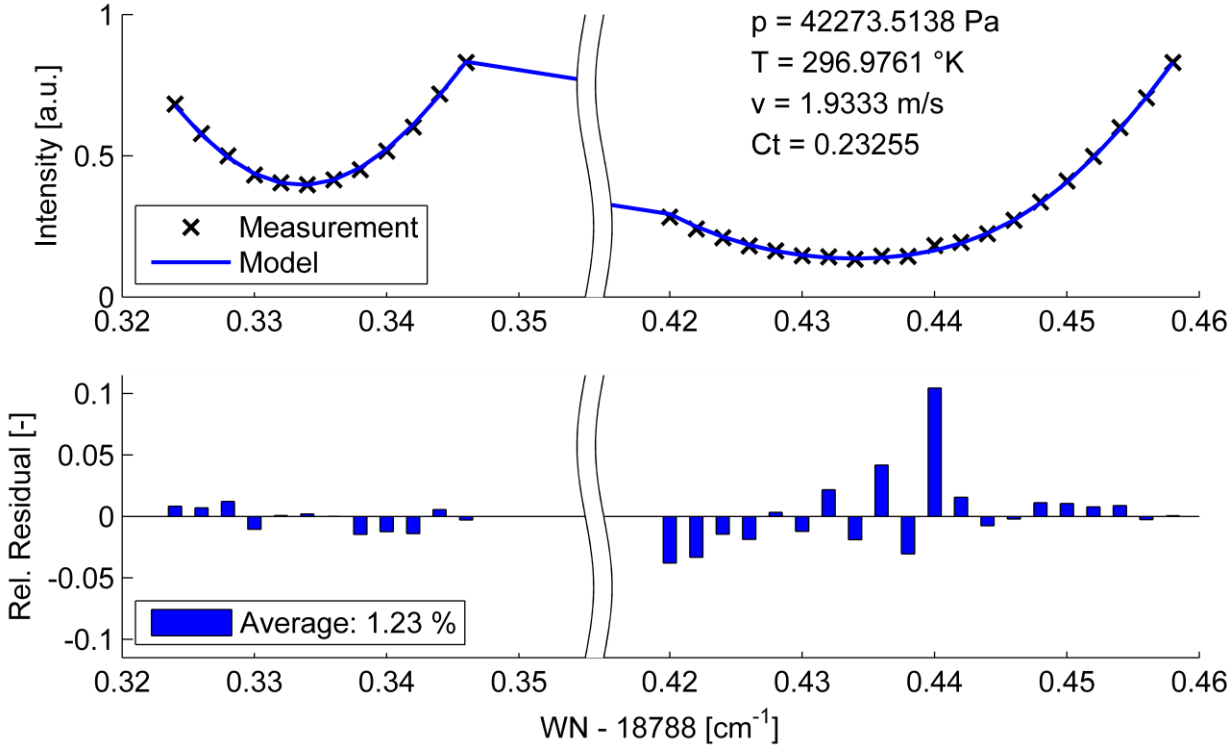

Fig 10 Vortex tube data are successfully evaluated using the Tenti model including full pressure sensitivity. While the residuals still show some systematic behavior, the results as well as the overall residual of 1.2% are well within the expected range considering the hardware not being designed for FRS.

The third aspect is about the applicability of the used Rayleigh model. While the Tenti S6 model was originally conceived for diatomic gases (and air as a mixture of these), it works for SF_6 as well due to its similar dipole moment - to an unknown degree, so an analytical model will be derived from data acquired with the same hardware at static conditions. To match the required range of the similarity parameter $y = 0.5...0.85$ pressure is varied from $p = 330...550$ mbar. While

the structural design of the model is still derived from the Tenti S6 model based on eleven parameters, each of these parameters is now assigned to its own arbitrary function and fitted to the calibration data (Doll, 2016). For SF6 within the given *y*-range the result is a set of 48 parameters.

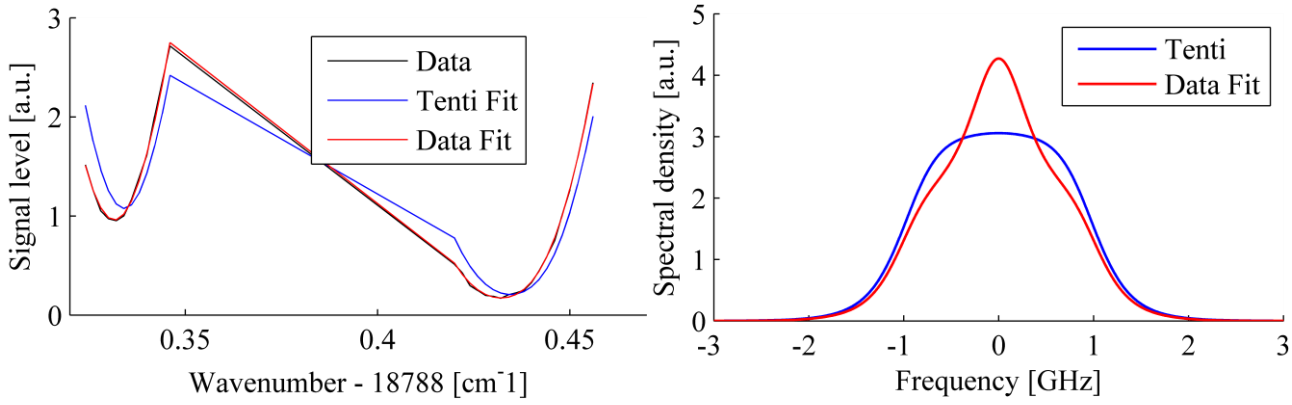

Fig 11 While the calibrated analytical model images the measured data very well (left), the solution is not unique due to the underdetermined character of the parameter set. The result is a significant deviation from physical line shapes (right), as shown for $y = 0.648$.

Considering the quality of the data fit (Fig 11, left) with an overall residual of 0.84 % the calibration is considered to be successful. Due to the amount of arbitrary parameters however the fit is not unique, thus while the model is the best representation of the Rayleigh profile as convoluted by the iodine cell, it does not necessarily match the actual physical line shape (Fig 11, right), in this case even less than with other documented data (e.g. Doll, 2016). Under these circumstances some follow-up questions arise: (i) Which hardware dependent effects are captured by the model, and how well can it be transferred to another FRS setup? (ii) Is the assumed *y*-similarity of the Tenti-model (Tenti, 1974) still valid? (iii) How numerically stable does a nonlinear regression based on this model converge towards its unique solution?

An indication for the latter two is gained by comparing an evaluation based on the calibrated model to one based on Tenti's model; for this purpose the same data point as in Fig. 11 is evaluated again. While the regression still converges numerically, the overall residual is almost unchanged (Fig. 12). This is true for the FSM as well as the combined method. Thus it has to be concluded that in this case transferring the model - which is still an ideal image of its calibration data - to the conditions of the presented measurement data does not yield any benefit rectifying the loss of proximity to the physical 'truth'.

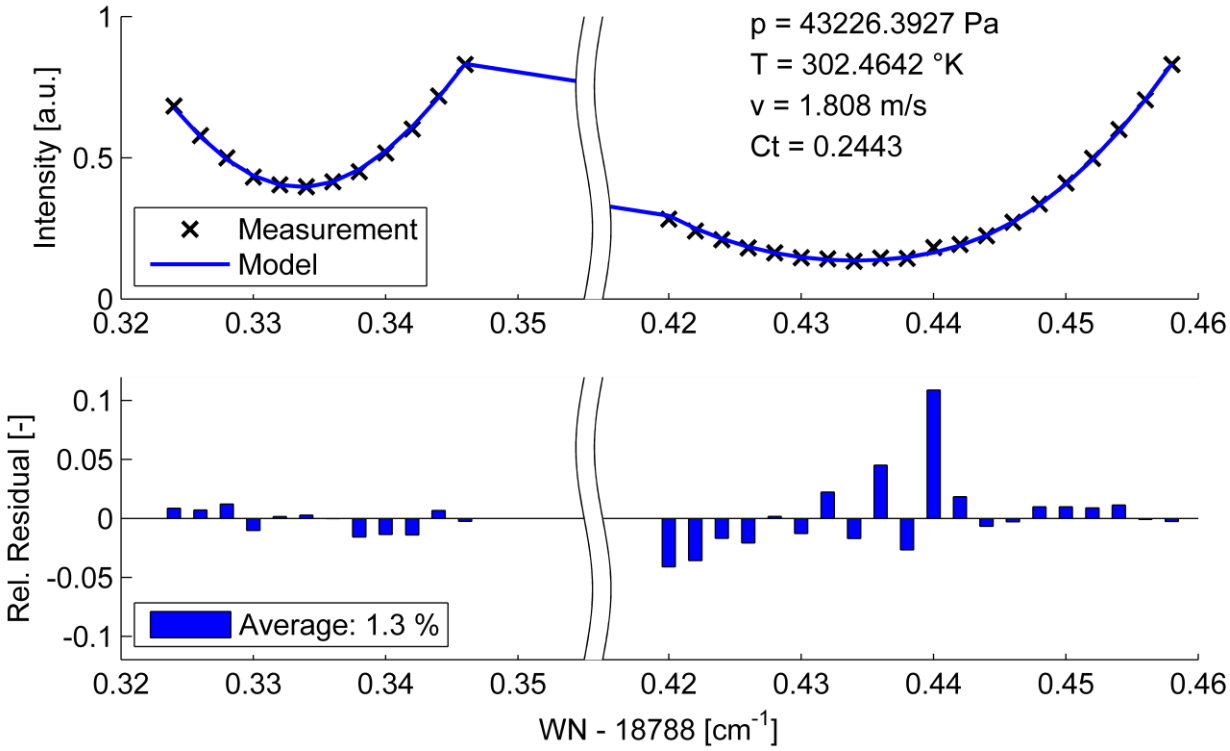

Fig 12 While the results are almost identical when using the calibrated model (bar plot, bottom), the overall residual is even slightly increased, compared to the Tenti-based evaluation (Fig. 10). Thus the numerical model does not yield any advantage.

To have a look at the transferability of numerical models a set of measurement data in air at the same RHVT position was evaluated with Tenti's model successfully ($R_s = 1.45$; $y = 0.253$), however a calibrated model for air, based on data acquired by a quite different approach (planar measurements with y-variation via observation angle; Doll, 2016) failed to converge: for once the data are outside its validity range ($y = 0.68...1.22$), also some deviations due to hardware changes (such as the bandpass filter and the optical path through the iodine cell) should be expected.

Fig. 13 shows the interpolated flow field of SF_6 (Tenti, FSM). The top row of data points exhibit a strong residual as well as faulty results: due to the proximity to the tube (1.5 mm wall distance) significant background noise leaks through the optical mode filter. While this behavior may be improved with additional effort put into optical alignment, the general issue will remain. The other 5 rows on the other hand feature credible results. The radial velocity data (3rd plot) may be compared to (Burow, 2016; Fig. 4) considering the difference in scaling and the additional inner tube: while the axial velocity presented there is subject to projection errors, the valid vorticity

data of this sector also indicate a minor radial component directed inwards, decreasing towards the outlet (right) and tube center (bottom).

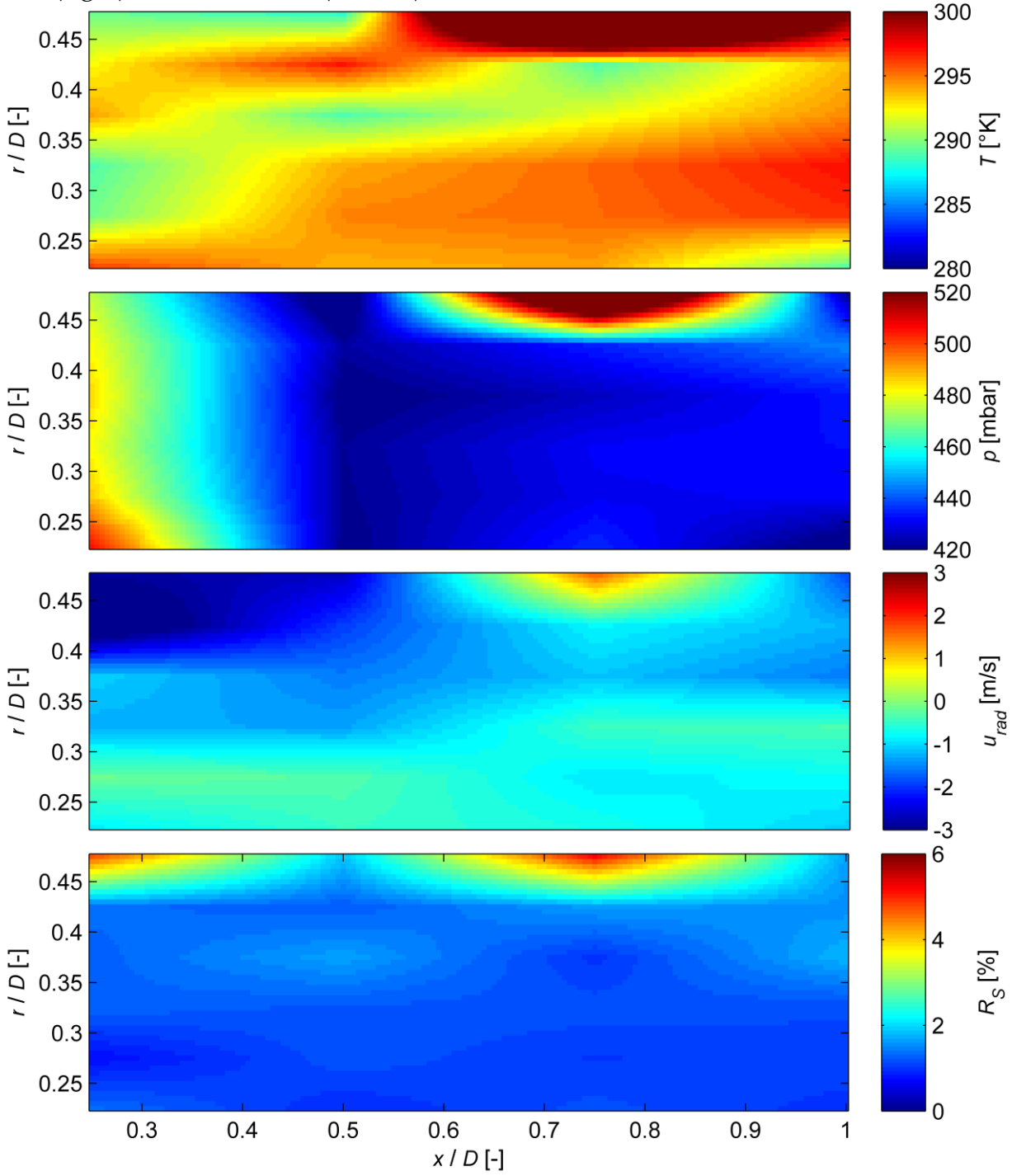

Fig 13 The 4 axial x 6 radial points measured in SF_6 are interpolated to allow comparing the results to other RHVT data. The residuals (bottom plot) suggest neglecting the outermost data points (top row) due to the strong influence of background reflections from the glass tube.

The temperature data on the other hand (1st plot) may be compared to (Doll, 2015; Fig. 5, top). Considering scaling, different inlet conditions (higher impulse), different medium (air) and the different setup (dual outlet RHVT instead of uniflow) a qualitative comparison still applies: temperatures in this sector are significantly decreased, however increasing with a distance from the inlet point. Considering an expected uncertainty of ~2 K single data points should not be read too much into. Last but not least for the pressure data (2nd plot) there are no reference data available, since uniflow vortex tubes in general serve more of an academic purpose, while it is used here only to allow for optical access from the inlet side. While the other dimensions are mostly unaffected by this distinction, pressure will differ significantly towards the wall on the left (missing cold outlet). Thus (again omitting the top data row close to the wall) the error in the pressure results stays unknown at this point.

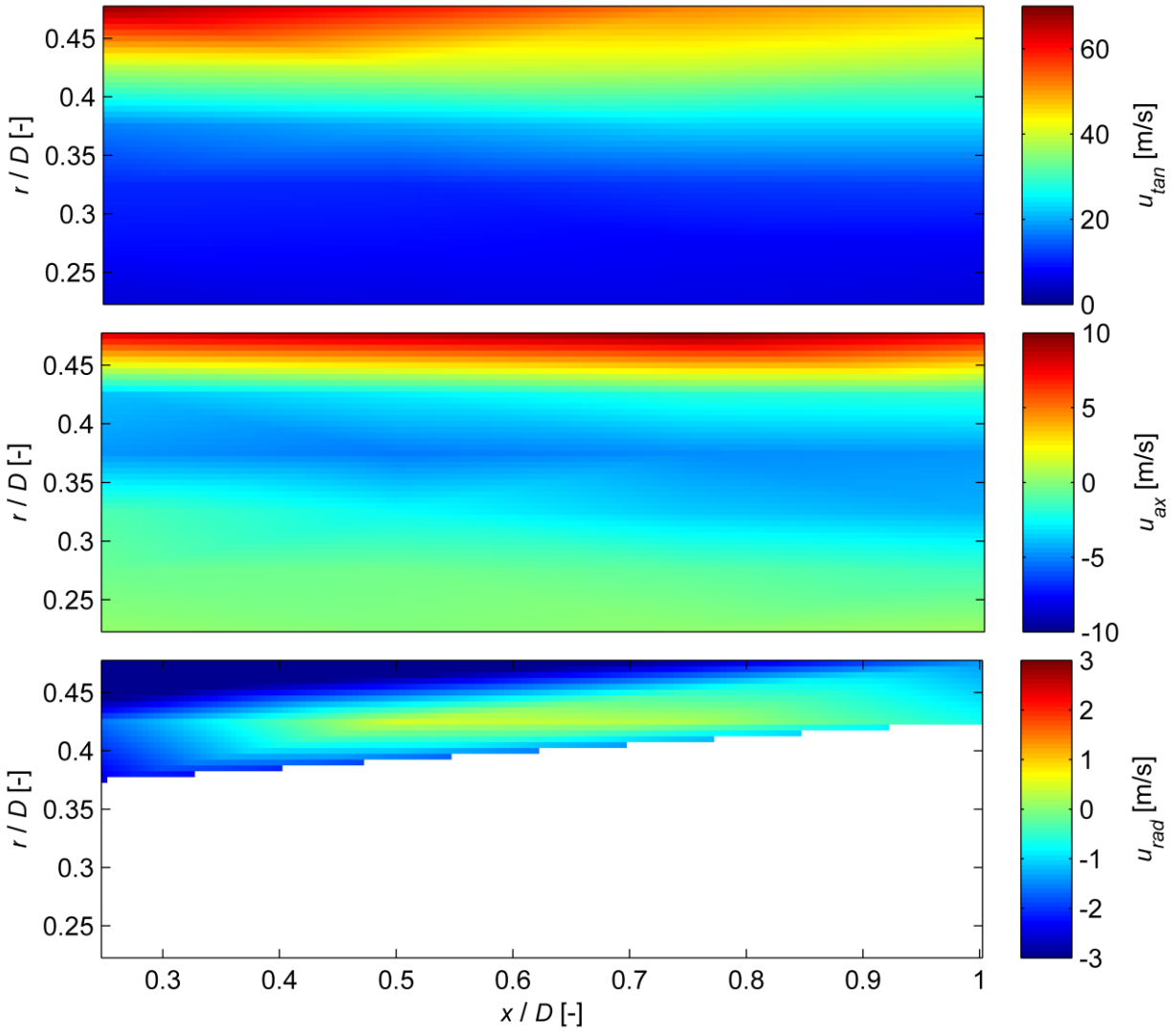

Fig 14 While the Doppler addition to L2F (bottom) is an established method, its applicability is limited for low velocity levels. The L2F data however for tangential (top) and axial (middle) velocities are consistent.

The value of FRS is often reduced to its temperature and pressure results, in cases like this however its velocity measurements are a valuable alternative to particle-wise DGV as an addition to L2F. DGV (Fig. 14, bottom) is limited in its applicability by two aspects: for once it suffers from background noise close to the wall as well (of the top row actually only two measurements were valid), but its dynamic range is limited as well. Considering the working principle of particle-wise DGV (Fig. 5), where a particle crossing the laser focus creates two quantitatively compared peaks with a temporal distance defined by the length of the delay fiber, these peaks may overlap at low velocity normal to the focus (< 30 m/s tangential), since the retention time of the particle within the focus exceeds the fiber delay. Since tangential velocity (Fig 14, top) scales with the radius, particle-wise DGV fails at smaller radii. Measurement uncertainties are similar to those of FRS, covering the deviation to the FRS data (Fig. 13).

The L2F data themselves (Fig 14, top: tangential / middle: axial velocity) are of good quality. The primary tangential rotation shows a decreasingly nonlinear radial distribution as well as steady dissipation during the precession towards the outlet as expected qualitatively (Doll, 2015), the spatial resolution however is insufficient for capturing small-scale acoustic features. Quantitatively the data also match PIV reference data (Fig. 15) very well; however these are available only for two radial positions.

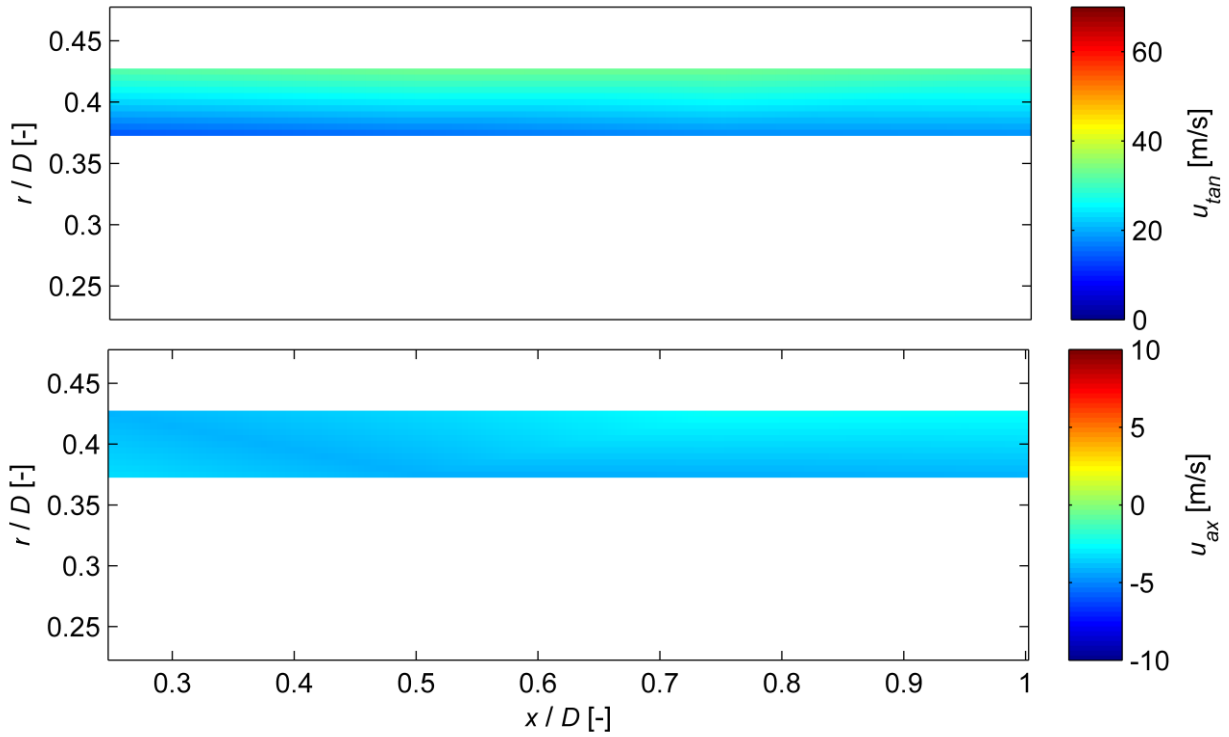

Fig 15 PIV reference data (same RHVT setup and parameters) for tangential and axial velocities are available as an excerpt from two tangential light sheets (measurement from outside the glass tube).

5 Conclusion

Based on previously acquired data the vortex tube setup was modified for testing endoscopic single-point measurement techniques. Data were acquired on the same optical hardware with Filtered Rayleigh Scattering (FRS), Laser-2-Focus (L2F) and particle-wise Doppler Global Velocimetry (DGV, spatially limited applicability). Successfully evaluated data were compared to each other where possible, as well as to literature and additional PIV data. Among different approaches to FRS evaluation the frequency scanning method based on Tenti's Rayleigh scattering model showed the most stable results.

While L2F and DGV have been used together as 3c-L2F successfully for some time now, the addition of FRS has been shown to deliver additional information on thermodynamics (p, T) as well as velocity. Thus it serves as an addition or substitute for particle-wise DGV, depending on the measurement task: while particle-wise DGV may not work for low velocity ranges, velocity uncertainties of FRS and scanning DGV are for the most part independent of absolute levels. On the other hand in a future step a combination of FRS and DGV may be able to grasp particle slip as well.

Considering the measurement schedule FRS and 3c-L2F are compatible as well. An L2F scan consists of several measurement points each with a duration of few seconds - same as FRS; using separate laser lines the angular L2F scan is optically independent of the frequency-wise FRS scan. Nonetheless two issues were raised concerning simultaneous measurements of FRS and 3c-L2F. First FRS data usually need to be referenced against the actual laser power within the region of interest (ROI); for the shown data the beam was accessed after passing through the ROI. This is usually not possible for actual endoscopic measurements, but sampling a reflection with an additional fiber may serve as a viable solution. More critical however is the issue of seeding induced fiber fluorescence cross-talk in the FRS signal. Since this aspect affects any fiber-based FRS measurements (single-point as well as planar), it offers an important research goal: while no immediate solution is at hand, approaches include: using large diameter multimode or hollow core fibers, substituting fiber technology in general, partial laser line filtering before the signal fiber, as well as numerical analysis and modelling of spectral vs. optical behavior of fiber bundles.

References

Burow E J, Doll U, Klinner J, Stockhausen G, Willert C (2016) Development of laser-optical measurement techniques on the vortex tube: Taking PIV to its limits. 18th Lisbon Symposium.

Doll U, Beversdorff M, Stockhausen G, Willert C, Schlüß D, Morsbach C (2014) Characterization of the flow field inside a Ranque-Hilsch vortex tube using filtered Rayleigh scattering, Laser-2-Focus velocimetry and numerical methods. 17th Lisbon Symposium.

Doll U, Burow E J, Beversdorff M, Stockhausen G, Willlert C (2015) The Flow Field inside a Ranque-Hilsch Vortex Tube Part I: Experimental Analysis using Planar Filtered Rayleigh Scattering. The ninth Symposium on Turbulence and Shear Flow Phenomena, Melbourne.

Doll U (2016) Gefilterte Rayleigh-Streuung zur simultanen Bestimmung von Druck-, Temperatur- und Geschwindigkeitsfeldern in Gasströmungen. PHD Thesis, TU Dresden.

Forkey J, Finkelstein N, Lempert W, Miles R (1996) Demonstration and characterization of filtered rayleigh scattering for planar velocity measurements. AIAA Journal 34 (3):442-448.

Förster W, Karpinsky G, Krain H, Röhle I, Schodl R (2000) 3 Component, Doppler Laser-Two-Focus Velocimetry Applied to a Transonic Centrifugal Compressor. 10th Lisbon Symposium.

Liew R, Zeegers J C H, Kuerten J G M, Michalek W R (2012) Maxwell's demon in the Ranque-Hilsch vortex tube. Physical Review Letters 109:054503.

Meyers J F, Komine H (1991) Doppler global velocimetry - A new way to look at velocity. Laser Anemometry - Advances and Applications 1:289-296.

Miles R B, Lempert W R, Forkey J N (2001) Laser Rayleigh scattering. Meas. Sci. Technol. 12:R33

Raffel M, Willlert C E, Scarano F, Kähler, C J, Wereley S T, Kompenhans J (2018) Particle Image Velocimetry - A Practical Guide. Springer, Berlin Heidelberg.

Röhle I (1999) Laser Doppler Velocimetry auf der Basis frequenzselektiver Absorption: Aufbau und Einsatz eines Doppler Global Velocimeters. PHD Thesis, Ruhr-Universität Bochum.

Schodl R (1980) A laser-two-focus (L2F) velocimeter for automatic flow vector measurements in the rotating components of turbomachines. Journal of Fluids Engineering, Transactions of the ASME 102 (4):412-419.

Tenti G, Boley C D, Desai R C (1974) On the Kinetic Model Description of Rayleigh-Brillouin Scattering from Molecular Gases. Canadian Journal of Physics 52 (4)

Udovic J A et al (2008) Spectral background and transmission characteristics of fiber optic imaging bundles. Appl Opt 47 (25):4560-4568.

Xue Y, Arjomandi M, Kelso R (2010) A critical review of temperature separation in a vortex tube. Experimental Thermal and Fluid Science 34 (8):1367-1374